Int. J. Heat Mass Transfer. Vol. 27, No. 12, pp. 2307–2319, 1984
Printed in Great Britain

0017 9310/84 $3.00 + 0.00
Pergamon Press Ltd.

Some new developments on coupled radiative–conductive heat transfer in glasses—experiments and modelling

T. KUNC, M. LALLEMAND and J. B. SAULNIER
Laboratoire de Thermique, E.N.S.M.A. et Laboratoire d'Energétique Solaire, C.N.R.S. 86034 Poitiers, France

(*Received* 20 *January* 1984)

Abstract—The difficulty in obtaining reliable phonic thermal conductivity of glasses at high temperature leads the authors to propose a methodology based on an experimental and numerical investigation, in order to separate the conductive and radiative part in a combined heat transfer in semi-transparent materials. The thermal conductimeter is composed of a guard plane plate and a Mach–Zehnder interferometer, supplying the total heat flux and the temperature distribution. With such a device no contacts are needed between sample and hot plate or heat sink. These measurements are treated numerically by a nodal analysis modelling of simultaneous conductive–radiative heat transfer. A monodimensional (non-diffusing) non-gray analysis including multireflections was considered. Determinations of the temperature derivative of the refractive index and the infrared spectra of materials at high temperature have been carried out. Values of the phonic conductivity of silica glass up to 900 K and borosilica glass up to 750 K for samples with different thicknesses and frontier's emissivities have been obtained by an identification process. Results are in agreement with literature data.

1. INTRODUCTION

HEAT transfer in semi-transparent materials (STM) at a high temperature results in a cooperation of heat exchange modes, namely conductive and radiative ones. Such coupled transfer is significant in numerous thermal engineering devices and metrology processes. This is the case for the manufacturing and processing of glasses, where the energetic balance and temperature distribution in tanks may be necessary, or for the growth of synthetic crystals from the melt. In the same way the vitrification process of nuclear wastes implies the knowledge of heat exchange capability between the glassy medium and its environment. Likewise, problems associated with thermal behaviour of optical windows under high radiative flux, re-entry of space vehicles, require a rigorous analysis of combined heat exchanges, often including the possibility of temperature dependence of thermophysical properties of the material.

Glasses, especially vitreous silica, because of their high chemical stability, good dielectric properties and relatively low cost, present great interest from a metrological point of view, since they can be used as standards in measurements of thermal conductivity. However, the presence of a radiative contribution within the total heat flux implies that, what is usually designed by conductivity, in the sense of Fourier law, is no longer an intrinsic property of the material, as it depends, for instance, upon the thickness of the sample, and upon the emissivity of the boundaries.

A better understanding of the phonon–phonon interaction in disordered systems, will be possible, when data concerning the true phonic thermal conductivity in non-crystalline solids will be available at high temperature. Then it may be possible to answer the remaining question: why is the temperature dependence of thermal conductivity in the vitreous state so radically different from that in the crystalline material of the same chemical composition.

Progresses in simultaneous conduction–radiation heat transfer problem in an absorbing–emitting medium (but non-scattering) have been obtained mainly from theoretical analysis in the case of the one-dimensional (1-D) scheme; up to now, experimental works have been a minority.

The 1-D non-linear problem of a slab of gray medium has been solved iteratively by Viskanta and Grosh [1]; the Schuster–Schwarchild–Chandrasekhar method [2] of discrete ordinates (discrete directions of propagation) was used by Anderson and Viskanta [3] for a non-gray medium the spectral properties of which were described by a multiband model. Other studies about combined radiative–conductive heat transfer analysis were summarized up to 1975 by Viskanta and Anderson [4] and up to the present by Viskanta [5].

Recently one of us [6] improved and developed a nodal analysis (zoning method) proposed previously by Hottel and Sarofim [7]. Such a method enabled an extensive numerical calculation to be made both in the steady and transient state of the complex thermal exchanges in SMT, for a system bounded by black frontiers, including conduction, convection, radiation phenomena in gray and non-gray media containing possible internal sources.

The experimental aspect was treated by Nishimura *et al.* [8] who measured the temperature distribution in a layer of molten glass, using thermocouples embedded in the melt. Eryou *et al.* [9] determined temperature and heat flux profiles within a layer of molten glass, with Planck numbers having an order of magnitude of about one. An optical method was used by these authors based on the knowledge of attenuation by temperature of a He–Ne laser beam. Viskanta *et al.* [10] and

NOMENCLATURE

a_{k,T_i} fractional spectral emissive power of spectral band k at nodal temperature T_i
C_i nodal heat capacity [J kg^{-1} K^{-1}]
d thickness of layer [m]
$E_n(x)$ exponential integral function (order n),

$$\int_0^1 \mu^{n-2} \, e^{-x/\mu} \, d\mu$$

F_{ij} view factor relative to surfaces S_i and S_j
G_{ij} conduction conductance
G_{ij}^r radiative conductance
k_c phonic thermal conductivity [W m^{-1} K^{-1}]
k_{eff} effective thermal conductivity [W m^{-1} K^{-1}]
L geometric length crossed by the laser beam inside the sample
m total number of spectral band
n refractive index
n_k refractive index relative to the spectral band k
dn/dT temperature derivative of refractive index [K^{-1}]
N total number of nodes
q_i local source term
q_r radiative heat flux along x
q_t total heat flux along x
S_i radiative surface relative to node i
S_{ij} exchange area between nodes i and j
$\overline{(S_iS_j)}$, $\overline{(S_iV_j)}$, $\overline{(V_iV_j)}$ extended exchange surface
$\overline{(s_is_j)}$, $\overline{(s_iv_j)}$, $\overline{(v_iv_j)}$ direct exchange surface
$\overline{(S_iS_j)}_k$, $\overline{(S_iV_j)}_k$, $\overline{(V_iV_j)}_k$ extended exchange area relative to spectral band k
$\overline{(s_is_j)}_k$, $\overline{(s_iv_j)}_k$, $\overline{(v_iv_j)}_k$ direct exchange area relative to spectral band k
ΔS difference of interference order
T temperature [K]
T_i nodal temperature [K]
T_g glassy transformation temperature [K]
V_i volume relative to node i
x_{ij} distance separating node i from node j
Δx uniform internodal distance.

Greek symbols
α linear thermal expansion coefficient [K^{-1}]
ε_i emissivity of gray surface S_i
κ_k absorption coefficient relative to spectral band k
λ wavelength of laser source
ρ_i diffuse reflectivity of gray surface S_i
σ Stefan–Boltzmann constant
ϕ_i^c nodal conductive heat flux
ϕ_i^r nodal radiative heat flux.

Anderson [11] in the case of a flat layer with different radiative boundary characteristics compared local temperature and total heat flux with predictions furnished by the rigorous 1-D radiative analysis. Men and Sergeev [12] used an algorithm to obtain the variation of the true thermal conductivity coefficient of fused silica with the temperature from experimental effective conductivity data. Hayes *et al.* [13] investigated thermal conductivity of infrared transparent chalcogenide glasses by a simplified approach of the radiative contribution.

The phonic thermal conductivity of vitreous silica and Pyrex at high temperature have been compiled by Powell *et al.* [14]. Effective thermal conductivity data and 'radiative thermal conductivity' correction relative to glasses of various composition in the vitreous state and smelt have been reviewed by Blazek and coworkers [15, 16].

The lack of reliable phonic thermal conductivity determinations of glasses at high temperatures leads the present authors to propose here an experimental and numerical approach in order to separate conductive and radiative contributions in a combined heat transfer. An attempt was made to test the method on fused silica and borosilica glasses at elevated temperatures (up to 950 K for the former and 750 K for the latter). Effects of the variation of the sample thickness and the radiative boundary conditions have been examined.

The experimental system used is composed of a guard plane plate heat fluxmeter in association with a Mach–Zehnder interferometer for supplying the temperature distribution along a prescribed direction into the slab. These measurements are then treated numerically by the nodal analysis based on a modelling of the simultaneous conductive and radiative heat transfer in a 1-D STM Realistic infrared absorption spectra (represented by a multi-band model) and multi-reflection phenomena have been taken into account. Accurate values of the phonic conductivity at various temperatures are achieved by separation of the two competing effects.

The infrared absorption spectra of vitreous silica and borosilica for glasses at high temperatures between 1 and 4.8 μm, and the temperature derivative of their refractive index at 0.6328 μm are presented in Section 2. In Section 3 a brief survey of the conductive–radiative transfer analysis in the scope of the nodal method is given, for a medium with different models of spectra and radiative boundary characteristics; Section 4 is devoted to describing the experimental facility; Section 5 displays the evolution of the effective conductivity measurements against temperature for the two types of glasses; the true thermal conductivity inferred by an

identification process is finally given in Section 6 with short comments on the results together with various sensible tests, against refractive index, absorption spectra models, and emissivity of the frontiers.

2. INFRARED ABSORPTION SPECTRA AND TEMPERATURE DERIVATIVE OF REFRACTIVE INDEX FOR FUSED SILICA AND BOROSILICA GLASSES AT HIGH TEMPERATURE

In an absorbing–emitting medium at high temperature an accurate determination of the near infrared absorption spectrum is needed to evaluate the radiative heat transfer contribution, in order to separate conductive and radiative effects. For example, as we shall see later, the assumption of a semi-gray medium in a borosilica glass involves an error larger than 9% for the phonic conductivity at 730 K. So, it appears necessary to carry out the determination of the absorption spectra of each material and possibly its evolution with temperature if these data are missing.

Knowledge of the thermo-optic coefficient dn/dT of the glass with temperature at the working wavelength and thermal expansion coefficient α are also needed when using the interferrometric method to evaluate quantitatively the temperature profile set up in the slab.

2.1. *Silica glass*

Specimens of silica glass were purchased from Heraeus Company (Suprasil quality). For this material there are extensive absorption data available between 1 and 4.8 μm in a temperature range up to 1370 K [17–21]. The spectrum used in this work is represented in Fig. 1 at 673, 873 and 1073 K for the wavelength range usable in radiative transfer at moderate temperatures.

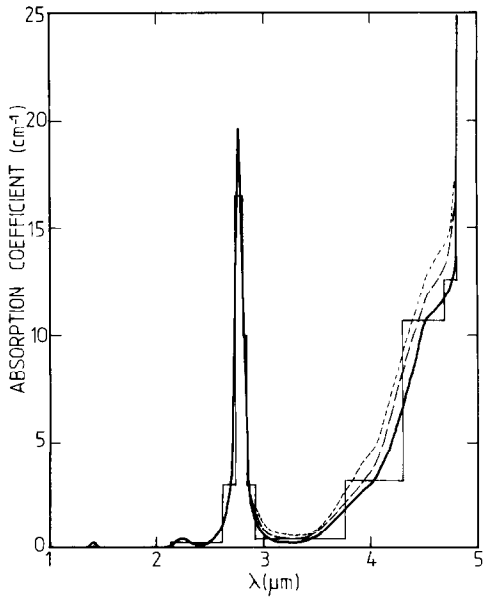

FIG. 1. Absorption coefficient of silica glass (Suprasil) and its eleven multi-band model: ——, $T = 673$ K; — —, $T = 873$ K; – – – –, $T = 1073$ K.

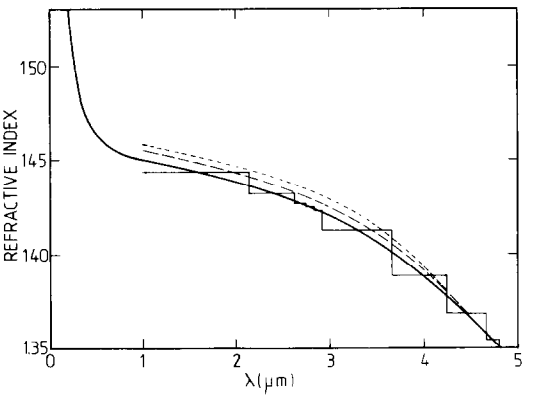

FIG. 2. Refractive index of silica glass (Suprasil) and its eleven multi-band model: ——, $T = 293$ K; — —, $T = 873$ K; – – – –, $T = 1073$ K.

For the 2.2–3.5 μm, and 3.5–4.8 μm ranges which have an important contribution to radiative transfer near 1000 K, data were taken from Edwards [17] and Petrov and Stepanov [21], respectively.

The spectra display three absorption bands, one located at 1.4 μm, two others at 2.23 and 2.75 μm attributed to fused quartz to hydroxyl radical, the latter having strong intensity in usual quality materials. Between 4.0 and 4.8 μm an increase of the absorption due to vibrational modes of stretching and flexion of the SiO_4 group begins. Beyond 4.8 μm vitreous silica can be considered as opaque in current thermal uses. It can be noticed in Fig. 1 that an increase in temperature produces a general rise of the absorption spectra, which is especially marked near the base wings of the two main peaks, and a shift of the opacity frontier toward the low wavelength range. From these data, the multiband infrared spectrum model introduced in the nodal analysis consists of a defined number of rectangular boxes, the height of which is fixed by a frequency average over the considered spectral interval. Bands in the vicinity of the 2.23 and 2.75 μm peaks are assumed to be temperature independent; intermediate bands are of variable height according to the temperature level.

The dispersion curve of the refractive index of fused silica taken from ref. [21] is represented on Fig. 2 at room temperature, 873 and 1073 K and is considered to be constant for each absorption band.

2.2. *Borosilica glass*

Samples of borosilica glass were purchased from Schott Company (BK7 grade). Because of a lack of information concerning the absorption spectra in the infrared for that glass, we had to perform its measurement at several temperatures.

A modified Perkin–Elmer monochromator model 98 was used. For a fixed temperature the absorption coefficient was deduced from an in and out method, by means of two optical cells containing a sample of different thickness embedded in a metallic furnace enclosed in a evacuated chamber. The spectra are plotted on Fig. 3 for room temperature and 770 K. It

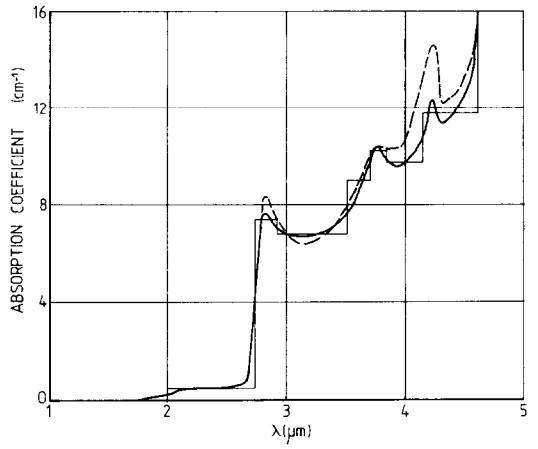

FIG. 3. Absorption coefficient of borosilicate glass and its nine multi-band model: ——, $T = 293$ K; — —, $T = 770$ K.

appears that the transparent region is sharply interrupted by the water band situated near 2.8 μm; beyond that value a region of semi-transparence follows, showing two others peaks at 3.7 and 4.25 μm. Like fused silica the medium can be considered opaque beyond 4.6 μm. It will be noticed that between 2.8 and 4.6 μm an increase of temperature has various effects on the absorption coefficient depending on the spectral position. However, the general trend may be considered for borosilica glass as a slight increase of the absorption especially in the long wavelength range. The multiband model introduced in the analysis is also represented in Fig. 3. Its refractive index is taken as constant all over the spectral range and equal to 1.5 [22].

2.3. *Temperature derivative of the refractive index of fused silica and borosilica glass*

A quantitative determination of the temperature field within the slab by an interferrometric method requires data on the temperature derivative of the refractive index of the material at the wavelength of the source [23]. For both glasses we performed the measurements of this coefficient for 0.6328 μm. The Fizeau interferrometer used for these determinations was described in a previous paper [24]; temperatures reached were 873 K for fused silica and 750 K for the borosilica, this limit being due to the vicinity of vitreous transformation temperature (T_g). The following linear law was retained: for vitreous silica [24]

$$(\mathrm{d}n/\mathrm{d}T) = 9.7 \pm 0.3 \times 10^{-6} + 0.95 \times 10^{-8}(T(\mathrm{K}) - 293)$$

and for borosilica glass [25]

$$(\mathrm{d}n/\mathrm{d}T) = 2.0 \pm 0.2 \times 10^{-6} + 0.63 \times 10^{-8}(T(\mathrm{K}) - 293).$$

Values obtained for vitreous silica differ somewhat slightly from those of Wray and Neu [26] measured by an absolute prism method and used by Anderson and Viskanta [3] for their experimental temperature profile determination. They are in agreement with more recent data by Gustavson and Karawacki [27].

For borosilica glass our values also agree with those published by the manufacturer near room temperature. Unfortunately, no reliable $\mathrm{d}n/\mathrm{d}T$ data was available for this material at higher temperatures. Furthermore, measurements should be stopped near 750 K because of the drastic variation of the optical path due partly to the abrupt rise of the thermal expansion coefficient of the material and partly to the important increase of the thermooptic coefficient itself beyond T_g.

As a consequence of the linear dependence of coefficient $\mathrm{d}n/\mathrm{d}T$ and α [22] on temperature of both materials, for the Mach–Zehnder interferometer, the temperature deviation associated with an interfrange is also dependent on the temperature level.

3. THE MODELLING OF THE COUPLED HEAT TRANSFER IN STM BY THE NODAL METHOD

We shall consider the case of an infinite slab of STM (excluding diffusion of radiation), limited by two isothermal parallel opaque walls, diffusively emitting, of prescribed temperature T_1 and T_2 respectively, for the hot one and for the cold one (Fig. 4). The temperature and heat flux distribution within the layer can be calculated by the nodal method both for a gray absorption spectrum (without spectral effect) and a non-gray one. In the nodal model, presented here, multireflexions of light path due to the presence of non-black frontiers, may also be taken into account.

3.1. *The nodal method applied to the gray case*

The nodal analysis considers that the system to be represented, is divided into small *isothermal* volumes (here slabs of finite thickness), the center of which is called a *node*, labelled i. The heat capacity C_i of such a node is easy to evaluate, and the possible external heat flux applied within the volume corresponding to node i will be represented by the source q_i.

In these conditions each node can exchange energy either by conduction or by radiation (more generally by convection also), for the conductive phenomenon with its nearer neighbours, and with all other nodes for the radiative phenomenon. So the energy balance equation can be written for the node i as

$$C_i \frac{\mathrm{d}T_i}{\mathrm{d}t} = \phi_i^c + \phi_i^r + q_i. \qquad (1)$$

When applied to nodes i and j, the Fourier law

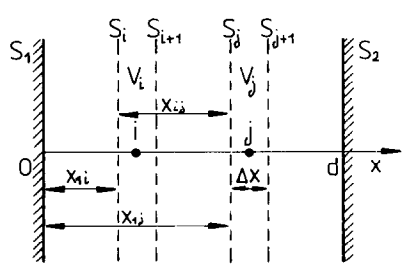

FIG. 4. Infinite slab of STM modelling by zone method.

expresses the conductive flux as

$$\phi_i^c = \sum_j G_{ij}(T_j - T_i) \tag{2}$$

with the summation index $j = i-1,\ i+1$ only. Straightforward calculations lead in the present case to the following expression for the conduction conductance

$$G_{ij} = k_c \frac{S_{ij}}{x_{ij}}. \tag{3}$$

An extension of the flux–temperature relation, equation (2), to the radiative transfer provides the general expression for the radiative conductance

$$G_{ij}^r = g_{ij}^r (T_i^2 + T_j^2)(T_i + T_j). \tag{4}$$

In the case of a black cavity with fully transparent medium and without internal reflexions g_{ij}^r is just given by

$$g_{ij}^r = n^2 \sigma S_i F_{ij} \tag{5}$$

where F_{ij} is the view factor relative to surfaces S_i and S_j; the term $S_i F_{ij}$ is called the 'exchange surface'.

The formulation of a thermal problem by the nodal method generally leads to the resolution of a set of non-linear differential (transient case) or algebraic (steady state) equations. Thanks to the appropriate software packages (SINDA, ENSMATHERM) this resolution is now particularly easy [6].

3.2. *The nodal model for a gray medium and black frontiers*

For a gray medium the classical concept of radiative conductance G_{ij}^r remains valuable, but the coefficient g_{ij}^r has to be re-expressed. In an absorbing emitting gray medium characterized by an absorption coefficient κ the usual view factor (see Hottel and Sarofim [7]) can be extended. With the help of the energy conservation principle [6], the final expressions of the exchange surfaces $(\overline{s_i s_j})\ (\overline{s_i v_j})\ (\overline{v_i v_j}) = g_{ij}^r / n^2 \sigma$ are given by Table 1.

Then for the steady-state problem applied to SMT of unitary section, with uniform internodal distance Δx, we only have to solve the non-linear algebraic equations issued from equations (1), (2) and (4) which can be written for node i

$$\frac{k_c}{\Delta x}(T_{i+1} + T_{i-1} - 2T_i) + \sigma n^2 \left(\sum_{j=2}^{N-1} (\overline{v_i v_j})(T_j^4 - T_i^4) + (\overline{s_1 v_i})(T_1^4 - T_i^4) + (\overline{s_2 v_i})(T_2^4 - T_i^4) \right) = 0 \tag{6}$$

or finally an equation of the form

$$\alpha T_i^4 + \beta T_i + \gamma = 0. \tag{7}$$

3.3 *The nodal model for a non-gray medium with black frontiers*

For a non-gray medium, for which spectral dependence of the absorption coefficient can be represented by a set of rectangular boxes (that means the medium is piece-wise gray) the concept of radiative conductance is now irrelevant [28]. However, by indentifying the local radiative flux to an impressed source (cf. the term q_i in equation (1)), the spectral dependence of the problem can be included in the nodal model. The impressed source q_i just depends on all the nodal temperatures, which makes the algebra a bit more non-linear. The evaluation of term q_i leads to the following expression

$$q_i = \sum_{k=1}^{m} \sigma n_k^2 \left\{ \sum_{j=2}^{N-1} (\overline{v_i v_j})_k (a_{k,T_j} T_j^4 - a_{k,T_i} T_i^4) + (\overline{s_1 v_i})_k (a_{k,T_1} T_1^4 - a_{k,T_i} T_i^4) + (\overline{s_2 v_i})_k (a_{k,T_2} T_2^4 - a_{k,T_i} T_i^4) \right\} \tag{8}$$

where the index j runs over the different node of the system, and the index k over the different bands of the model of absorption spectra.

The different non-gray exchange surfaces $(\overline{v_i v_j})_k$, $(\overline{s_1 v_j})_k$ appearing in the above equation being re-expressed from those of Table 1 by solely changing the gray value κ with the value κ_k of the absorption coefficient for the rectangular band k.

Let us observe that in equation (8) we need the fractional spectral emissive power a_{k,T_j} which represents the fraction of energy emitted by a black body of temperature T_j associated with the emission over the band k. Because $a_{k,T_i} \neq a_{k,T_j}$ it can be seen why the notion of radiative conductance cannot be used for the non-gray problem.

3.4. *The nodal analysis for a non-gray medium with reflective frontiers*

The boundaries surfaces are now assumed to be gray and diffusely reflecting (emissivity ε_i, reflectivity $\rho_i = 1 - \varepsilon_i$).

When multireflexions of radiations are taken into account, Hottel and Sarofim [7] gave the expressions of

Table 1

Exchange surface symbols	Surfaces implied	Exchange surfaces for a unit surface
$(\overline{s_1 s_2})$	boundary–boundary	$2E_3(\kappa d)$
$(\overline{s_1 v_j})$	boundary–medium	$2(E_3(\kappa x_{1,j}) - E_3(\kappa x_{1,j+1}))$
$(\overline{v_i v_j})$	medium–medium	$2(E_3(\kappa x_{i,j+1}) - E_3(\kappa x_{ij}) - E_3(\kappa x_{i+1,j+1}) + E_3(\kappa x_{i+1,j}))$

extended exchange surfaces $(\overline{V_iV_j})$, $(\overline{S_1V_i})$, $(\overline{S_2V_i})$, implied now in equation (8) and which are connected to the direct exchange surfaces $(\overline{v_iv_j})$, $(\overline{s_1v_i})$ and $(\overline{s_2v_i})$. In Appendix A the relations between these two sets of factors are presented in the frame of the Gebhart theory of multireflexions in an enclosure filled with a gray SMT and then extended in Appendix B to the case where a non-gray medium is involved in the radiative transfer. In Appendices A and B are also given the expressions of the source term q_i entering into the energy equation (1) in presence of multireflexions when the medium is considered as gray and non-gray, respectively.

4. EXPERIMENT

The experimental device is essentially composed of a guard plane heater acting as a heat fluxmeter and a Mach–Zehnder interferometer allowing visualization of the temperature field setting up across the glass layer.

4.1. *The heat fluxmeter*

On Fig. 5 is represented a layout of the fluxmeter. It is constituted by the following elements: a pile of thick copper plates (a) engraved to receive a 'Thermocoax' wire heater. On the upper plate, isolated from the others by small cylindric pieces of alumina (b) is settled the central plate of the heat fluxmeter (c); in order to compensate the lateral heat losses a guard plate (d) is fitted around it. When the temperatures are balanced between that of the central heater (c), on the one hand with the temperature of its support (a) and on the other hand with that of the guard, the balancing electric power feeding the central plate measures the total heat flux emitted. The heat sink (e) is sustained at some few millimeters above the heated surface; whatever the temperatures of the hot plate are its own temperature is regulated within $\pm 0.1°C$ near room temperature by a water circulation thermostat (f). The glass samples (g) of the same area as the fluxmeter are positioned on the top of three thermocouples (h), which also measure the temperature of the sample's hot face. With this arrangement no contact between specimen of glasses and the plates is necessary. A metallic shield (i) is fixed perpendicularly on the guard plate matching closely the temperature at the edges of the sample. Several other shields (j) surround the apparatus but leaving a viewport for light transmission.

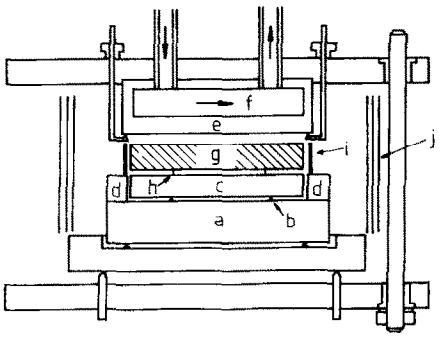

FIG. 5. The heat fluxmeter: (a) heat plate; (b) alumina; (c) heat fluxmeter; (d) guard plate; (e) cold plate; (f) circulation thermostat; (g) glass sample; (h) thermocouples; (i), (j) metallic shield.

On both hot and cold plates several thermocouples are soldered and are connected, via a multiplexer to an automatic voltmeter controlled by a video system which acquires all the electrical information.

The different heaters are fed separately by a controlled power supply which performs automatically the balance of temperature between the different heat plates.

4.2. *The interferometer*

The thermo-conductimeter is placed in a secondary vacuum chamber to avoid convective losses. This chamber is included in the measurement arm of a Mach–Zehnder interferometer. The light source is a 5 mW He–Ne laser, the beam of which is first treated by a space filter and then expanded to reach approximately a diameter of 30 mm.

After running through the sample, the (re)combination of the measurement and the reference beams, produces an interferogram which allows the visualization of the temperature field inside the glass layer.

The principal interest of this contactless technique is to give a more accurate temperature difference across the sample, than the conventional sandwich assembly of current thermo-conductimeter. Moreover, the sample here being free of external mechanical constraint, it cannot be damaged by stresses imposed by large temperature gradient.

The main drawbacks of the interferometric thermo-conductimeter is the need of a necessary preliminary accurate knowledge of the thermooptic coefficient dn/dT and of the linear thermal expansion coefficients, and furthermore as already underlined it limits the temperature range of the experiment to before the glassy transition temperature.

4.3. *Samples*

The glass samples are parallelepipedic, with a section of 70×65 mm, and with various thicknesses 6, 10, 15 and 20 mm, allowing a suitable length to thickness ratio. The two opposite faces perpendicular to the light beam are polished to $\lambda/5$ and parallel to within 2 fringes cm^{-1}. In all experiments the part of the basic surfaces facing the hot or cold plates are covered with a black paint (Sperex SP 100) the total hemispherical emissivity of which has been measured up to 650°C by means of the heat fluxmeter. Emissivity measurements are comprised between 0.85 at 200°C and 0.92 at 650°C. The black paint has shown, during the experiments, good adhesive properties on both glasses even at high temperature. We also prepared samples with mirror boundaries thanks to a vacuum evaporated aluminium layer, which was finally recovered with black paint. The

edges of thick samples are also mirror boundaries, that make them of infinite extent.

4.4 *Temperature profile determination*

Let us consider the Mach–Zehnder interferometer [23]. If x represents the abscissa in a direction perpendicular to the beam (and co-linear to the impressed temperature gradient, Fig. 4), the temperature difference $\Delta T(x)$ associated with a difference of interference order $\Delta S(x)$ is given by the expression

$$\Delta T(x) = \frac{\lambda}{L}\left(\frac{\mathrm{d}n}{\mathrm{d}T} + (n-1)\alpha\right)^{-1} \Delta S(x). \qquad (9)$$

At steady state two methods for counting the fringes were used. Either the projection of the magnified interferogram on a screen where the number and fractional number of fringes were directly evaluated, or the record of the interferogram on a film; both methods produce the same uncertainty. For a 15 mm thick sample $\mathrm{d}\Delta S/\Delta S$ it is about 1% for a large temperature gradient and 2% for a low gradient.

4.5. *Accuracy*

Taking into account the precision on $\mathrm{d}n/\mathrm{d}T$ and α, the relative error for the temperature difference between the hot and cold face of a sample is about $\pm 3\%$ for fused silica and $\pm 6\%$ for the borosilica glass. The resulting total inaccuracy on heat flux measurement can be estimated at 3%, so the precision on the effective thermal conductivity is about $\pm 6\%$ for fused silica and $\pm 9\%$ for borosilica.

5. RESULTS

Two typical interferograms, obtained at steady state for an infinite fringe field are shown on Figs. 6(a) and (b). A fused silica sample hot surface was heated at 983 K, the cold one at 892.7 K; for borosilica glass the two temperatures were 753 and 701.9 K, respectively. The fringe pattern present is of a high density for the former, due to the strong impressed thermal gradient, and of a moderate density for the second. They display a direct picture of the isotherm configuration along the thickness of the layers. In Fig. 7 is plotted the temperature profile deduced from relation (9) for the interferogram (Fig. 6(a)); it shows a quasi-linear distribution except in the very vicinity of the edges where a slight increase of fringe density can be observed due to the high temperature gradient near the boundaries. The measured departure from linearity is 0.66 K in the cold region and 1.95 K in the hot region. For fused silica, with the same temperature conditions as above, the temperature profile calculated by the nodal method (20 nodes) and an emissivity surface of 0.9 is also represented on Fig. 7; it can be seen that the general shape of the experimental temperature distribution is reproduced, in agreement with the conductive–radiative transfer modelling. However, the deviation of the numerical profile from linearity is slightly more accentuated near the cold zone than in the hot one.

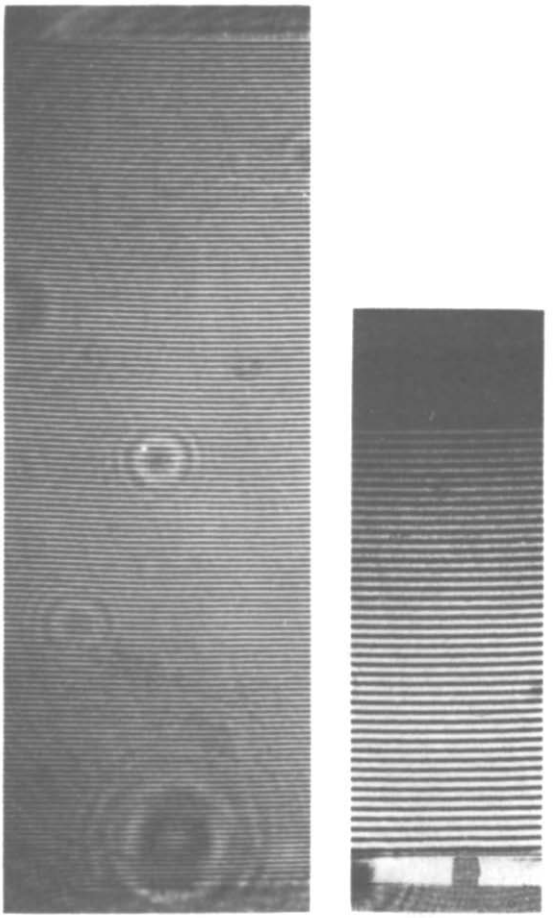

(a) (b)

FIG. 6. Typical steady state interferograms. (a) Silica glass: $T_1 = 983$ K; $T_2 = 892.7$ K; $d = 20$ mm. (b) Borosilicate glass: $T_1 = 753$ K; $T_2 = 701.9$ K; $d = 15.2$ mm.

Let q_t be the total heat flux density (experimentally measured) and ΔT the corresponding temperature difference between the two opposite surfaces of the studied sample (thickness d). One can usually define an effective thermal conductivity by

$$k_{\mathrm{eff}} = |q_t/(\Delta T/d)|. \qquad (10)$$

As we know, this quantity is not an intrinsic property of the material when we are dealing with a combined heat transfer, as it depends on the temperature level, the thickness of the sample, its surface emissivities and its shape. However, from our experimental point of view this k_{eff} is yet pertinent.

The variations of k_{eff} against temperature are presented on Fig. 8 for a 10 and 20 mm thick fused silica sample, up to 950 K on Fig. 9 for a 6 and 15 mm borosilica glass sample with high emissivity boundaries, and on Fig. 10 for mirror boundaries, up to 730 K. It is observed for each material that from 570 K, experimental data are distributed following different curves corresponding to each sample. The scattering of

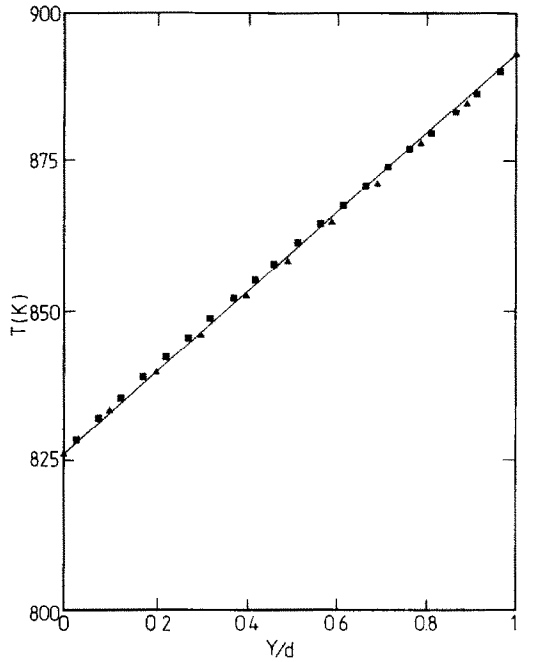

FIG. 7. Temperature profile in silica glass: ▲, experiment; ■, nodal analysis (20 nodes); ——, linear profile.

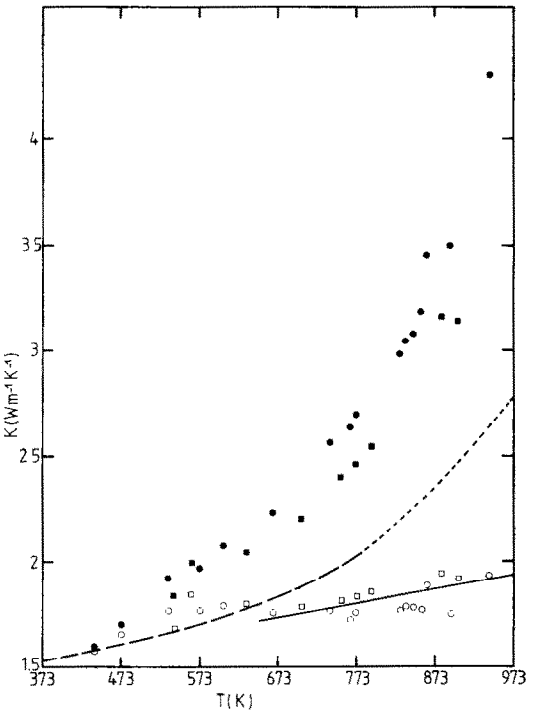

FIG. 8. Thermal conductivity of silica glass. Experiment: ●, 20 mm thickness; ■, 10 mm thickness. Phonic conductivity: ○, 20 mm thickness; □, 10 mm thickness. Literature: — —, Sugawara [32]; ——, Men and Chechel'nitsky [31]; ——, recommended values by Powell *et al.* [14].

measurements can be partly attributed to the different experimental conditions (the imposed temperature gradient being 45 K cm^{-1} at 950 K but only 4 K cm^{-1} at 470 K), and partly to experimental errors.

For fused quartz (Fig. 8) the experimental curve for the 20 mm specimen is in good agreement at 720 K with those of Chechel'nitsky [29] with the same sample thickness and for 'elevated emissivity' of surfaces. At lower temperature, data of this author differ from ours by about −8% near 570 K. Above 720 K our values are in agreement with those of Anderson and Viskanta [3] for their 12.7 mm specimen; but their data are higher between 570 and 720 K.

The evolution with respect to temperature of the effective conductivity of borosilica glass shows a similar behaviour. However, the magnitude of the effect is always lower than for fused silica even in the case of nearly black frontiers. It shows up to 730 K a quite sensitive influence of the thickness, when similar emissivity boundaries are used and a noticeable emissivity effect, at constant thickness, when passing from $\varepsilon \simeq 0.90$ to 0.05. Unfortunately, for this glass no comparison of k_{eff} is possible with data of the literature.

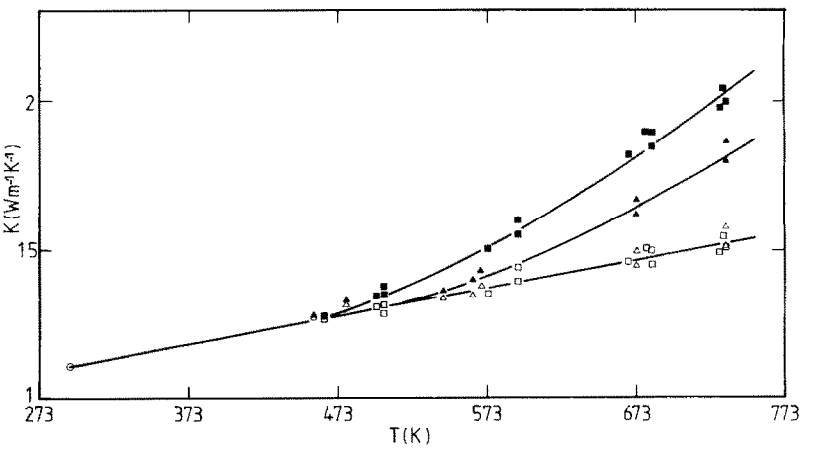

FIG. 9. Thermal conductivity of borosilicate glass. Experiment: ■, 15.2 mm thickness; ▲, 6 mm thickness. Phonic conductivity: □, 15.2 mm thickness; △, 6 mm thickness. Literature: ○, Schott [22].

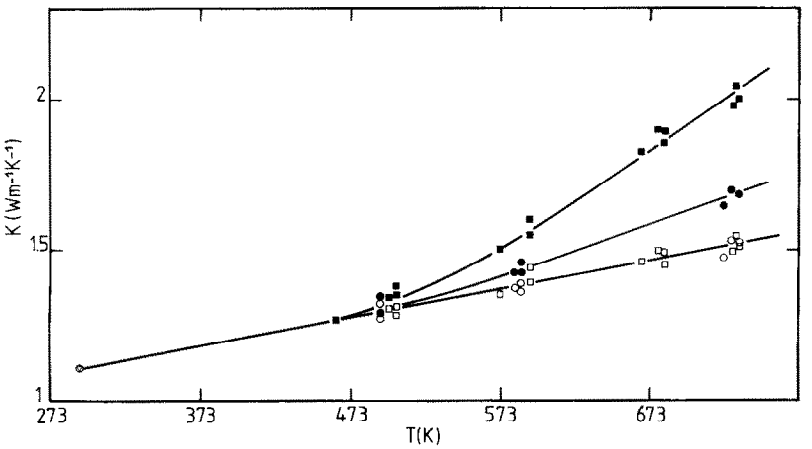

FIG. 10. Surface emissivity effects on thermal conductivity of borosilicate glass (15.2 mm thickness). Experiment: ■, high emissivity surfaces ($\varepsilon = 0.9$); ●, low emissivity surfaces ($\varepsilon = 0.05$). Phonic conductivity: □, $\varepsilon = 0.9$; ○, $\varepsilon = 0.05$.

6. IDENTIFICATION OF THE PHONIC CONDUCTIVITY

6.1. *The identification method*

We are now in a position to carry out the determination of the thermal conductivity of a SMT at high temperature. In fact, for a fixed temperature of the SMT slab, we know its surface emissivity, its spectral internal absorption coefficient and spectral refractive index; we are also in possession for a defined thickness, of the temperature profile and of the total density heat flux across the sample. So we can connect these data and results with the thermal model issued from the nodal analysis and then use a classical identification approach in order to deduce the phonic conductivity of a semi-transparent material.

Starting from an initial guess of the thermal conductivity k_{c1}, the corresponding temperature profile and density of radiative heat flux are calculated with the nodal model. Let us design these first two results by $T(k_{c1},j)$ and $q_r(k_{c1},j)$, respectively. Because the sensitivity to k_c is stronger for the flux than for the temperature, we can choose for the second step of the iteration a new conductivity coefficient such as

$$k_{c2} = \frac{1}{N}\sum_{j=1}^{N}(q_t - q_r(k_{c1},j))/(T(k_{c1},j) - T(k_{c1},j+1))/\Delta x \quad (11)$$

where q_t is the known experimental value of the total density heat flux and $q_r(k_{c1},j)$ the radiative heat flux over the different nodes j relative to the temperature profile $T(k_{c1},j)$.

The iterative process will be stopped after the ith step when for example

$$\frac{|k_{c,i} - k_{c,i-1}|}{k_{c,i-1}} < 0.01. \quad (12)$$

We established that the proposed method has a very fast convergence, since only three iterations are generally sufficient to satisfy the numerical criterion (12). In the most complex radiative situation, i.e. including multireflexions, the time required to identity a phonic conductivity coefficient is about 10 min on a Norsk Data 100 minicomputer.

6.2. *Thermal conductivity of fused silica*

The thermal conductivity of fused silica was inferred from the two effective conductivity curves in the case of an eleven band model whose absorption spectra and refractive index curve are given in Figs. 1 and 2. The evolution with temperature of the two samples is presented up to 950 K on Fig. 8. We can verify that values obtained from experiments for different material thicknesses agree within 6% in the high temperature region. We also notice that effective and phonic thermal conductivity curves deviate one from the other about 470 K, the true conductivity curve presenting a monotonous linear increase, although the apparent conductivity one rises at a fast rate, the ratio of their magnitudes reaching a factor of 3 near 1000 K.

As a comparison are also reproduced on Fig. 8 some data of literature selected for minimizing the radiative transfer contribution. Wray and Connelly reported measurements obtained with a hot wire transient technique on fused silica up to 2100 K [30]; Men and Chechel'nitsky [31] and Sugawara [32] used samples sandwiched between low emissivity metallic surfaces, for which conductive transfer is dominant. The agreement between our results and these previous measurements is quite good up to 620 K; for higher temperatures, data of Sugawara and Men and Chechel'nitsky diverge, both displaying an increase of k_c with temperature but their curves having opposite concavity; at 720 K their data differ by about 9%. Our values fall between these two curves, closest to those of Sugawara below 600 K and approaching those of Men and Chechel'nitsky above 600 K. At 1000 K a 10% difference is observed with the data of Wray and Connelly calculated as a mean value over several runs of their work. We can notice that the N.B.S.

recommended values of thermal conductivity of fused quartz are about 40% higher than the present results at 1000 K, due probably to the non-elimination of radiative transfer participation.

6.3. *Borosilica glasses*

The thermal conductivity of borosilica glasses deduced from our experiments for black and mirror boundaries (specular boundaries are treated here as diffuse ones, the rigorous analysis is in development) presents also a slight linear increase when the temperature rises (Fig. 9). The extrapolation of our results near room temperature gives a value of 1.11 W $m^{-1} K^{-1}$ in excellent agreement with the data of the BK7 manufacturer. Data obtained for the two different sample thicknesses and different emissivities are comparable within 6%.

The behaviour of k_c for that glass is very similar with that found by Champomier [33] with the hot wire technique for float glasses—a soda lime silica—up to 770 K. Other comparisons are possible with results on Pyrex glass—a borosilica; recommended N.B.S.'s values differ only slightly from ours at low temperature and by 9% at 700 K.

6.4. *Sensitivity against to several physical parameters*

Further aspects concerning the sensitivity of the model and consequently of the computed thermal conductivity, with respect to variations of the physical input parameters are to be examined; especially those of the infrared spectral model of absorption, refractive index spectral model and radiative properties of the boundaries (emissivity).

6.4.1. *Tests on absorption spectra models.* The experimental absorption spectra may serve to define several box models. Instead of the refined realistic nine rectangular band model of the borosilica glass leading to the results on k_c given in Section 6.3 a simpler spectral model consisting, for example, of only three bands: transparency from visible to 2 μm, semi-transparent between 2 and 4.6 μm ($\kappa = 660$ m^{-1}) and opaque beyond 4.6 μm, may be introduced in the nodal analysis. The resulting effect in the identification of k_c, then, gives at 730 K a value which deviates by 9% from those for the more realistic model.

For fused silica the simplification consisting in a division of the infrared spectra into six bands rather than eleven as in Section 6.2, leads at 940 K to a difference in k_c of about 10%. In the same way considering the eleven band model at 1000 K, by lowering only from $\kappa = 80$ to 70 m^{-1} the weak band comprised between 2.94 and 3.73 μm, which corresponds to the region of the maximum Planck function at 940 K, implies a decrease of k_c at this temperature of only 2%. As this change in absorption coefficient of the most temperature sensitive band is weak, it can be possible in the case of vitreous silica to neglect the temperature dependence of the spectra for the determination of thermal conductivity. When taking into account the temperature dependence of the spectra of the borosilica glass, again only a slight difference is observed. In that case, although there is a significant variation of the radiative flux contribution for each band, the total null effect is due to an algebraic cancelling out of the various band deviations.

6.4.2. *Tests on refractive index model.* The dispersive properties of the refractive index of fused silica refractive in the near infrared are well known up to 4.8 μm and they are summarized by Petrov and Stepanov [21], they vary smoothly between 1.452 at 1 μm to 1.354 at 4.64 μm as shown on Fig. 3. Calculations of k_c in Section 6.2 were made by assigning for each band of the absorption spectra a constant refractive index value n_k which closely approaches the dispersive curve. The thermal conductivity at 940 K of fused silica has been recalculated in the case of a uniform value of n over the useful spectral region, namely $n_k = 1.43$ for $k = 1$–11, all others physical parameters remaining the same. In such conditions a decrease of 14% of k_c has been obtained.

It seems that this occurrence is not general since several glasses, for instance, window glass [34], have a refractive index with only small variations in the near infrared up to 4.8 μm. For borosilica glass it seems correct to take a single refractive index value for radiative transfer modelling.

6.4.3. *Tests on surface emissivity.* Determination of thermal conductivity of fused silica has been performed for surfaces with diffusely gray emissivity, $\varepsilon = 0.9$ and for black frontiers. At 940 K for emissivity $\varepsilon = 1$ the increase of the radiative transfer with respect to the case when $\varepsilon = 0.9$ is severe; the conductive contribution is thus lowered and the inferred phonic conductivity decreased by about 15%.

7. CONCLUSION

In a combined radiative and conductive heat transfer in STM, the two contributions may be separated by means of the application of a one-dimensional nodal modelization associated with the experimental determination of the temperature profile and the total heat flux density. The method has been applied with success to silica and borosilica glasses at elevated temperatures. Even in situations when radiative effects are dominant—black emissivity frontiers, high thickness, temperature above 700 K—the true phonic thermal conductivity was identified for both materials with reasonable accuracy.

It has been shown that a preliminary extensive knowledge of the infrared optical properties of the materials was necessary, if not, the accumulation of neglected effects will bring out quite erroneous determinations.

Finally if conducting experiments for samples with low emissivity boundaries, small enough thickness and by taking into account the multireflexion phenomena—thus minimizing radiative participation, the method could be used to deduce the true phonic

conductivity of semi-transparent materials at high temperatures.

REFERENCES

1. R. Viskanta and R. J. Grosh, Heat transfer by simultaneous conduction and radiation in an absorbing medium, *Trans. Am. Soc. Mech. Engrs*, Series C, *J. Heat Transfer* **84**, 729–734 (1962).
2. S. Chandrasekhar, *Radiative Transfer*. Dover, New York (1960).
3. E. E. Anderson and R. Viskanta, Spectral and boundary effects on coupled conduction. Radiation heat transfer through semi-transparent solids, *Wärme- und Stoffübertragung* **1**, 14–24 (1973).
4. R. Viskanta and E. E. Anderson, Heat transfer in semi-transparent solids, *Adv. Heat Transfer* **11**, 317–441 (1975).
5. R. Viskanta, Radiation heat transfer: interaction with conduction and convection and approximate methods in radiation, 7th Int. Heat Transfer Conf., München, Vol. 1, pp. 103–121 (1982).
6. J. B. Saulnier, La Modélisation Thermique et ses Applications aux Transferts Couplés et au Contrôle Actif, Thèse de Doctorat d'Etat, Université de Poitiers (1980); J. B. Saulnier et J. Martinet, Le Verre et la Thermocinétique des Matériaux Semi-Transparents, *Rev. Phys. Appl.* **15**, 175–182 (1980).
7. H. C. Hottel and A. F. Sarofim, *Radiative Transfer*. McGraw-Hill, New York (1967).
8. M. Nishimura, M. Hasatami and S. Sugiyama, Simultaneous heat transfer by radiation and conduction at high temperature. One dimensional heat transfer in molten glass, *Int. Chem. Engng* **8**(4), 739–745 (1968).
9. N. D. Eryou and L. R. Gliksman, An experimental and analytical study of radiative and conductive heat transfer in molten glass, *Trans. Am. Soc. Mech. Engrs*, Series C, *J. Heat Transfer* **94**, 224–230 (1972).
10. R. Viskanta, E. E. Anderson and W. H. Stevenson, Heat transfer through semi-transparent solids, *Trans. Am. Soc. Mech. Engrs*, Series C, *J. Heat Transfer* **95**, 179–186 (1973).
11. E. E. Anderson, Combined conduction and radiation in semi-transparent solids, Thesis Purdue University (1972).
12. A. A. Men and O. A. Sergeev, Investigation of thermal conductivity, thermal diffusivity, and emittance of semi-transparent materials at high temperatures, 3rd Conf. on Thermophysical Properties, Turin 1972, *High Temp. High Press.* **5**, 19–28 (1972).
13. D. I. Hayes, S. N. Rea and A. R. Hilton, Thermal conductivity of infrared transparent chalcogenide glasses *J. Am. Ceram. Soc.* **58**(3–4), 135–137 (1975).
14. R. W. Powell, C. Y. Ho and P. E. Liley, Thermal conductivity, NSRDS-NBS **8**, 69 (1966); Y. S. Touloukian and D. P. De Witt, *Thermal Conductivity—Non Metallic Solids*. IFI/Plenum, New York (1970).
15. A. Blazek and J. Endrys, Review of thermal conductivity data, Part. II: thermal conductivity at high temperatures, Int. Comm. Glass. Sub. Committee A5 (1981).
16. A. Blazek, Thermal conductivity of glasses and method of determination, *Silikaty* **25**(4), 359–381 (1981).
17. O. E. Edwards, Optical transmittance of fused silica and elevated temperatures, *J. Opt. Soc. Am.* **56**(10), 1314–1319 (1966).
18. I. H. Malitson, Interspecimen comparison of the refractive index of fused silica, *J. Opt. Soc. Am.* **55**, 1205–1209 (1965).
19. A. V. Vanyushin and V. A. Petrov, Investigation of the spectral absorption coefficient of quartz glasses in the 2.0–4.8 μm region at high temperatures, *Teplofiz. Vys. Temp.* **14**(3), 661–663 (1976).
20. E. C. Beder, C. D. Bass and W. L. Shackleford, Transmissivity and absorption of fused quartz between 0.22 and 3.5 μm from room temperature to 1500°C, *Appl. Optics* **10**(10), 2263–2268 (1971).
21. V. A. Petrov and S. V. Stepanov, Radiation characteristics of quartz glasses spectral radiating power, *Teplofiz. Vys. Temp.* **13**(20), 335–345 (1975).
22. Schott Company, Catalog (1983).
23. W. Hauf and U. Grigull, Optical methods in heat transfer, *Adv. Heat Transfer* No. 6, 133–366 (1970).
24. M. Lallemand et J. Martinet, Influence de la Température sur le Coefficient Thermooptique dn/dT de Verre de Silicates Sodo-Calciques (floats) et du Verre de Silice, *Verres Réfract.* **35**(4), 675–680 (1981).
25. S. Sekkouti, Variation des Constantes Optiques d'un Verre de Borosilicate en Fonction de la Température, D.E.A., Université de Poitiers (1983).
26. J. H. Wray and J. T. Neu, Refractive index of several glasses as a function of wavelength and temperature, *J. Opt. Soc. Am.* **59**(6), 774–776 (1969).
27. S. E. Gustavson and E. Karawacki, Refractive index measurements in fused $NaNO_3$ and KNO_3 by a modified thermooptic technique, *Appl. Optics* **14**, 1105–1110 (1975).
28. Y. Bertin, Développement d'un Logiciel de Calcul de Champ de Température dans un Milieu Semi-Transparent, D.E.A., Université de Poitiers (1982).
29. A. Z. Chechel'nitsky, On the thermal conductivity of fused quartz in the temperature range 350–1100 K, *Teplofiz. Vys. Temp.* **10**(2), 285–289 (1972).
30. K. L. Wray and T. J. Connoly, Thermal conductivity of clear fused silica at high temperatures, *Appl. Phys.* **10**(11), 1702–1705 (1959).
31. A. A. Men and A. Z. Chechel'nitsky, Thermal conductivity of fused quartz, *Teplofiz. Vys. Temp.* **11**(6), 1309–1312 (1973).
32. A. Sugawara, The precise determination of thermal conductivity of pure fused quartz, *J. Appl. Phys.* **39**(13), 5994–5997 (1968).
33. F. Champomier, cited in ref. [16].
34. C. K. Hseih and K. C. Su, Thermal radiative properties of glasses from 0.32 to 206 μm, *Solar Energy* **22**(1), 37–43 (1979).
35. B. Gebhart, *Heat Transfer*, pp. 117–122. McGraw-Hill, New York (1961).

APPENDIX A

THE GEBHART THEORY OF MULTIREFLEXIONS IN A GRAY MEDIUM

Radiative heat exchanges among surfaces diffusely reflecting, separated by a participating medium (i.e. emitting and absorbing) may be obtained starting from the well-known Gebhart theory [35] for cavities filled with a transparent medium.

Let us design by $(\overline{S_iS_j})$ the total exchange surface associated with surfaces S_i and S_j in a cavity composed of M such surfaces each characterized by a reflectivity ρ_i, and separated by a transparent medium. The Gebhart theory expresses a relation between the extended exchange surfaces and the direct exchange surfaces $(\overline{s_is_j})$ introduced in the main text. The Gebhart relations can be written as

$$(\overline{S_iS_j}) = \varepsilon_j(\overline{s_is_j}) + \sum_{l=1}^{M} \rho_l(\overline{s_is_l})(\overline{S_lS_j})/S_l. \tag{A1}$$

The first term on the RHS of the above equation represents the direct exchange between surfaces S_i and S_j leading to an absorption by S_j of flux emitted by S_i $((\overline{s_is_j}) = S_iF_{ij}$, F_{ij} being the view factor); in the second term $\rho_l(\overline{s_is_l})(\overline{S_lS_j})/S_l$ leads to an indirect transfer from S_i to S_j via reflecting surface S_l.

Extended exchange surfaces for a one-dimensional absorbing–emitting system enclosed by reflecting walls (Fig. 4) can be derived by simple energetic arguments from direct exchange surfaces.

For the direct exchange surfaces associated with radiative

transfer between surface and medium, it can be written [7]

$$\overline{(s_i v_j)} = \overline{(s_i s_j)} - \overline{(s_i s_{j+1})}; \qquad i = 1,2 \tag{A2}$$

and for those between medium and medium

$$\overline{(v_i v_j)} = \overline{(v_i s_j)} - \overline{(v_i s_{j+1})}. \tag{A3}$$

When multireflections are taken into account, similar relations can be obtained for extended exchange surfaces

$$\overline{(S_i V_j)} = \overline{(S_i S_j)} - \overline{(S_i S_{j+1})} \tag{A4}$$

and

$$\overline{(V_i V_j)} = \overline{(V_i S_j)} - \overline{(V_i S_{j+1})}. \tag{A5}$$

Letting each emissivity for the surfaces of internal nodes equal to 1 and so the corresponding reflectivity equal to zero, the Gebhart relations for a semi-transparent medium can be written by substituting equations (A1) and (A2) into equation (A4)

$$\overline{(S_i V_j)} = \overline{(s_i v_j)} + \sum_{l=1}^{2} \rho_l \overline{(s_i s_l)}\,\overline{(S_l V_j)}/S_l; \qquad i = 1,2 \tag{A6}$$

and in a similar way from equations (A3), (A5) and (A6)

$$\overline{(V_i V_j)} = \overline{(v_i v_j)} + \sum_{l=1}^{2} \rho_l \overline{(v_i s_l)}\,\overline{(S_l V_j)}/S_l. \tag{A7}$$

So, extended factors may be expressed from direct factors and reflectivity of surfaces.

From the above expressions it is easy to establish the extended exchange terms $\overline{(S_1 S_2)}$, $\overline{(S_1 V_i)}$, $\overline{(S_2 V_i)}$ and $\overline{(V_i V_j)}$ with respect to direct exchange surface terms. One obtains

$$\overline{(S_1 S_2)} = \frac{\varepsilon_2 \overline{(s_1 s_2)}}{1 - \rho_1 \rho_2 \overline{(s_1 s_2)}^2/(S_1 \cdot S_2)} \tag{A8}$$

$$\overline{(S_1 V_i)} = \frac{\overline{((s_1 v_i)} + \rho_2 \overline{(s_1 s_2)}\,(v_i s_2)/S_2)}{1 - \rho_1 \rho_2 \overline{(s_1 s_2)}^2/(S_1 \cdot S_2)} \tag{A9}$$

$$\begin{aligned}\overline{(V_i V_j)} = {} & \overline{(v_i v_j)} \\ & + \frac{\rho_1 \overline{(s_1 v_i)}}{S_1} \frac{\overline{(s_1 v_j)} + \rho_2 \overline{(s_1 s_2)}\,\overline{(s_2 v_j)}/S_2}{1 - \rho_1 \rho_2 \overline{(s_1 s_2)}^2/(S_1 \cdot S_2)} \\ & + \rho_2 \frac{\overline{(s_2 v_i)}}{S_2} \frac{\overline{(s_2 v_j)} + \rho_1 \overline{(s_1 s_2)}\,\overline{(s_1 v_j)}/S_1}{1 - \rho_1 \rho_2 \overline{(s_1 s_2)}^2/(S_1 \cdot S_2)}\end{aligned} \tag{A10}$$

where the expressions of the direct exchange surfaces can be taken from Table 1 of the main text.

Furthermore, the extended reciprocity relation can be written

$$\varepsilon_1 \overline{(S_1 V_i)} = \overline{(V_i S_1)}; \qquad \overline{(V_i V_j)} = \overline{(V_j V_i)}$$

and

$$\varepsilon_1 \overline{(S_1 S_2)} = \varepsilon_2 \overline{(S_2 S_1)}.$$

In these conditions at the steady state, the energy balance equation in a slab of gray material, for a given node i, can be written

$$k_c(T_{i+1} - T_{i-1} - 2T_i) + q_i = 0$$

where the source term may be expressed as

$$q_i = \sigma n^2 \left[\sum_{j=2}^{N-1} \overline{(V_i V_j)}(T_i^4 - T_j^4) + \varepsilon_1 \overline{(S_1 V_i)}(T_1^4 - T_i^4) + \varepsilon_2 \overline{(S_2 V_i)}(T_2^4 - T_i^4) \right] \tag{A11}$$

still allowing the use of 'radiative conductance' concept.

APPENDIX B

EXPRESSION OF THE SOURCE TERM q_i FOR A NON-GRAY MEDIUM ENCLOSED IN A SLAB WITH MULTIREFLECTIONS

When multireflections are present in an enclosure composed of several diffusely reflecting surfaces of emissivity $(\varepsilon_1, \varepsilon_2, \ldots, \varepsilon_i \ldots)$ and containing a non-gray participating medium which absorption spectra may be represented by a box model, in the source term q_i appeared non-gray extended surfaces $\overline{(V_i V_j)}_k$, $\overline{(S_1 V_i)}_k$, $\overline{(S_2 V_i)}_k$, associated with each spectral band k. Besides the non-gray extended reciprocity relation becomes

$$\sum_{k=1}^{m} \varepsilon_1 a_{k,T_i} \overline{(S_1 S_i)}_k = \sum_{k=1}^{m} \varepsilon_i a_{k,T_i} \overline{(S_i S_1)}_k \tag{B1}$$

where a_{k,T_i} is the fractional emissive power at the nodal temperature T_i associated with band k.

The source term q_i for a slab bounded by surfaces S_1 and S_2 of respective emissivity ε_1 and ε_2 may now be written

$$\begin{aligned} q_i = \sum_{k=1}^{m} \sigma n_k^2 \Big\{ & \sum_{j=2}^{N-1} \overline{(V_i V_j)}_k (a_{k,T_j} T_j^4 - a_{k,T_i} T_i^4) \\ & + \varepsilon_1 \overline{(S_1 V_i)}_k a_{k,T_1} T_1^4 - \overline{(V_i S_1)}_k a_{k,T_i} T_i^4 \\ & + \varepsilon_2 \overline{(S_2 V_i)}_k a_{k,T_2} T_2^4 - \overline{(V_i S_2)}_k a_{k,T_i} T_i^4 \Big\} \end{aligned} \tag{B2}$$

but the following expression holds

$$\sum_{k=1}^{m} n_k^2 a_{k,T_i} \overline{(V_i S_1)}_k = \sum_{k=1}^{m} n_k^2 a_{k,T_i} (\overline{(S_i S_1)}_k - \overline{(S_{i+1} S_1)}_k) \tag{B3}$$

which from equation (B1) is equal to

$$\sum_{k=1}^{m} \varepsilon_1 n_k^2 a_{k,T_i} (\overline{(S_1 S_i)}_k - \overline{(S_1 S_{i+1})}_k)$$

or

$$\sum_{k=1}^{m} \varepsilon_1 n_k^2 a_{k,T_i} \overline{(S_1 V_i)}_k.$$

In these conditions

$$\begin{aligned} q_i = \sum_{k=1}^{m} \sigma n_k^2 \Big\{ & \sum_{j=2}^{N-1} \overline{(V_i V_j)}_k (a_{k,T_j} T_j^4 - a_{k,T_i} T_i^4) \\ & + \varepsilon_1 \overline{(S_1 V_i)}_k (a_{k,T_1} T_1^4 - a_{k,T_i} T_i^4) \\ & + \varepsilon_2 \overline{(S_2 V_i)}_k (a_{k,T_2} T_2^4 - a_{k,T_i} T_i^4) \Big\} \end{aligned} \tag{B4}$$

which generalizes equation (8) when the emissivity of boundaries are different from one.

QUELQUES DEVELOPPEMENTS NOUVEAUX SUR LE TRANSFERT DE CHALEUR COUPLE CONDUCTION-RAYONNEMENT DANS LES VERRES: EXPERIENCE ET MODELISATION

Résumé—La difficulté d'obtenir des valeurs fiables de la conductivité thermique des verres à haute température a conduit à proposer une méthodologie expérimentale et numérique permettant la séparation des effets conductif et radiatif dans un transfert de chaleur combiné dans un milieu semi-transparent. Le thermoconductimètre se compose d'une plaque plane gardée et d'un interféromètre Mach–Zehnder qui fournissent d'une part le flux de chaleur total et d'autre part la distribution de température. Au moyen d'un tel dispositif aucun contact n'est nécessaire entre l'échantillon et les plaques chaude ou froide. Les mesures sont ensuite traitées numériquement à l'aide de l'analyse nodale modélisant le transfert couplé conduction–radiation dans le cas monodimensionnel d'un milieu non gris (non diffusant), siège de multiréflexions. Des déterminations du coefficient de température de l'indice de réfraction et du spectre d'absorption infrarouge à haute température ont été effectuées. Les valeurs de la conductivitié phonique de la silice vitreuse jusque'à 900 K et d'un verre de borosilicate jusqu'à 750 K ont été obtenues par une méthode d'identification pour différentes valeurs d'épaisseur d'échantillons et d'émissivité aux frontières. Les résultats sont en accord avec ceux de la littérature.

NEUERE ERKENNTNISSE ZUR GEKOPPELTEN WÄRMEÜBERTRAGUNG DURCH STRAHLUNG UND LEITUNG IN GLÄSERN—EXPERIMENT UND THEORIE

Zusammenfassung—Die Schwierigkeit, die Wärmeleitfähigkeit von Gläsern bei hohen Temperaturen zuverlässig zu bestimmen, veranlaßt die Autoren, ein Verfahren vorzuschlagen, das auf experimentellen und numerischen Untersuchungen aufbaut und das Ziel hat, den überlagerten Wärmetransport in halbtransparenten Materialien in Wärmeleitung und Wärmestrahlung zu trennen. Die Wärmeleitfähigkeits-Meßeinrichtung besteht aus einer ebenen Schutzplatte und einem Mach–Zehnder-Interferometer zur Aufbringung der Wärmestromdichte und der Temperaturverteilung. Bei einer solchen Einrichtung besteht kein Kontakt zwischen der Meßprobe und der beheizten Platte oder der Wärmesenke. Die Messungen werden numerisch mit Hilfe eines Knotenmodells, welches den simultanen Wärmetransport durch Strahlung und Leitung berücksichtigt, ausgewertet. Eine eindimensionale (nicht streuende) Analyse, die Mehrfachreflexion berücksichtigt, wurde durchgeführt. Der Temperatureinfluß auf den Brechungsindex und auf das Infrarot-Spektrum von Materialien hoher Temperatur wurde bestimmt. Mit Hilfe eines Identifikationsverfahrens wurde die Wärmeleitfähigkeit von Silikatglas bis zu 900 K und die von Borsilikatglas bis zu 750 K für Proben von unterschiedlicher Dicke und Oberflächenemission bestimmt. Die Ergebnisse stimmen mit Literaturangaben überein.

НЕКОТОРЫЕ НОВЫЕ РАЗРАБОТКИ ВЗАИМОСВЯЗАННОГО ЛУЧИСТО-КОНДУКТИВНОГО ТЕПЛОПЕРЕНОСА В СТЕКЛАХ. ЭКСПЕРИМЕНТ И МОДЕЛИРОВАНИЕ

Аннотация—Трудность точного определения теплопроводности стекол при высоких температурах акустическим методом навела авторов на мысль предложить метод, основанный на экспериментальном и численном исследовании и заключающийся в разделении кондуктивной и лучистой компонент сложного теплопереноса в полупрозрачных материалах. Измеритель теплопроводности состоит из предохранительной плоской пластины и интерферометра Маха–Цендера, с помощью которого определяется величина суммарного теплового потока и распределение температур. При использовании такого прибора отсутствует контакт между образцом и нагретой пластиной или тепловым стоком. Результаты измерения обрабатываются численным методом на основе анализа узловых точек, моделирующих совместный кондуктивно-лучистый теплоперенос. Использован одномерный (недиффузионный) несерый подход с учетом многократных отражений. Определены температурная производная показателя преломления и инфракрасные спектры материалов при высоких температурах. Методом идентификации получены значения звуковой проводимости кремниевого стекла при температурах до 900 К и боросиликатного стекла до 750 К в образцах разной толщины и с разной граничной степенью черноты. Результаты согласуются с данными, имеющимися в литературе.